SciEn

Proceedings of 8th International Conference on Mechanical Engineering and Renewable Energy 2025
10-12 December, 2025, Chattogram, BANGLADESH

SciEn Conference Series: Engineering Vol. 4, 2026, pp 177-183 https://doi.org/10.38032/scse.2026.4.96

Albatross and Peregrine Falcon Flight Inspired Biomimetic Wing Design: A Comparison with NACA 23015

Anish Deb Turjo, Chandirma Deb, Mamjad Yousuf*

Department of Mechanical Engineering, Chittagong University of Engineering & Technology, Chattogram-4349, Bangladesh

ABSTRACT

Innovations in engineering, especially in the area of aerodynamics, have historically been inspired by nature. Birds have evolved incredibly effective wing structures that maximize lift, minimize drag, and enable adaptation to various flight circumstances. In this study, we combine several important aerodynamic traits from two amazing bird species to create a bioinspired wing: the Peregrine Falcon, the fastest bird in the world, which is renowned for its agility and capacity for high-speed maneuvers, and the Albatross, which is praised for its unmatched gliding efficiency. The 3D model of the wing was developed in Solidworks, meticulously integrating the high aspect ratio and tapered tips seen in the Albatross, alongside the swept-back design of the Peregrine Falcon. This model was then analyzed in ANSYS Fluent at a Reynolds number of 6×10^5 and an inlet velocity of 29.78 m/s, using the NACA 23015 wing as a reference. The results show that the Albatross & Falcon (A&F) wing peaked at an angle of 5°, while the NACA 23015 reached its maximum lift-to-drag ratio at 15°, showing a 33% gain in aerodynamic efficiency and a delayed stall beyond 15°. The pressure contours showed less flow separation and more efficient airflow. These findings imply that adding biomimetic components could greatly increase lift output and stability, creating chances for the creation of more nimble and fuel-efficient aircraft and UAV designs.

Keywords: Peregrine Falcon, Albatross, Bioinspired design, CFD simulation, NACA airfoil

1. Introduction

Nature has long been a major source of inspiration for engineers, particularly in the realm of aerodynamics. Birds have developed incredibly effective wing structures over millions of years that maximize lift, reduce drag, and adjust to different flying situations. The Peregrine Falcon [1] and Albatross [2] stand out among these bird species due to their remarkable flying skills. The albatross is well known for its gliding efficiency, which enables it to go great distances with little energy thanks to its long, thin wings and high aspect ratio. On the other hand, the Peregrine Falcon, one of the world's fastest birds [3], uses its swept-back wings to reach incredible speeds and perform precise aerial manoeuvres.

Engineers can create more effective wing structures for modern aircraft by researching and using these inherent flight properties. Because modern aviation seeks to attain high fuel efficiency without sacrificing flight speed, this project intends to design a biomimetic wing that combines the essential characteristics of both the Albatross and Peregrine Falcon. However, efficiency and performance are traded off in conventional aerofoil designs since improving one frequently results in a degradation of the other. However, nature demonstrates that both may coexist, which motivates the development of novel aerodynamic designs. SolidWorks was used to produce a 3D model of the wing, and ANSYS Fluent CFD simulations were used to assess the wing's aerodynamic performance. The biomimetic wing's performance was evaluated by comparing it to the NACA 23015 airfoil, a commonly used benchmark in aerodynamic research. The lift-to-drag ratio, lift and drag coefficients, stall behaviour at various angles of attack, and other significant aerodynamic parameters were investigated. The objective was to determine whether, in comparison to conventional aerofoil designs, a wing design inspired by nature could improve aerodynamic efficiency. Such biological efficiency has been tried to be replicated in artificial systems in earlier research. A Peregrine Falcon-inspired aerofoil was examined mathematically and experimentally by Yuvaraj et al. [1], who found that the lift-to-drag ratio increased by 12–15% when compared to traditional profiles. In a similar vein, Mathew et al. [4] shown that the Albatross's high aspect ratio wings greatly improve overall aerodynamic efficiency by reducing induced drag. Additionally, Zhang et al. [5] showed that adding a bird-inspired dihedral design improves unmanned aerial vehicle (UAV) flight stability and energy efficiency. Despite these developments, the majority of current research is on single species-inspired designs, ignoring the possible advantages of combining elements from several high-performance flyers.

The findings of this research contribute to the expanding area of biomimetic engineering and demonstrate its potential to enhance aircraft performance for improved stability, maneuverability, and fuel efficiency. This study expands our understanding of effective wing configurations and provides valuable insights for the future of eco-friendly aviation by applying biomimicry principles. The results may benefit commercial aircraft, unmanned aerial vehicles (UAVs), and other aerodynamic innovations that need to balance energy efficiency with flight performance.

2. Governing Equations

The Reynolds and Navier Stokes (RANS) equations, which include the continuity, momentum, and turbulence model equations, were solved to simulate the airflow interacting with the airfoil [6-7].
Continuity equation for mass conservation.

$$\frac{\partial \rho}{\partial t} + \frac{\partial(\rho u)}{\partial x} + \frac{\partial(\rho v)}{\partial y} = 0 \quad (1)$$

Where t represents time, u and v are components of velocity in the x and y directions, respectively and density is denoted by ρ.

Momentum equations are used to illustrate Newton's second law in relation to fluid motion:

$$\frac{Du}{Dt} = X - \frac{1}{\rho}\frac{\partial p}{\partial x} + \frac{\mu}{p}\left[\frac{\partial^2 u}{\partial x^2} + \frac{\partial^2 u}{\partial y^2} + \frac{\partial^2 u}{\partial z^2}\right]$$
$$\frac{Dv}{Dt} = Y - \frac{1}{\rho}\frac{\partial p}{\partial y} + \frac{\mu}{p}\left[\frac{\partial^2 v}{\partial x^2} + \frac{\partial^2 v}{\partial y^2} + \frac{\partial^2 v}{\partial z^2}\right] \quad (2)$$

where p and μ is static and dynamic viscosity respectively

k-ε turbulence model was used to close the RANS equations:

$$\frac{\partial \rho}{\partial t} + div\,(\rho u k) = div\left[\left(\mu_t + \frac{\rho \mu_t}{\sigma_k}\right) grad k\right] + \rho \mu_t G - \rho \varepsilon$$
$$\frac{\partial \rho \varepsilon}{\partial t} + div\,(\rho u \varepsilon) = div\left[\left(\mu_t + \frac{\rho \mu_t}{\sigma_\varepsilon}\right) grad \varepsilon\right] + C_{1\varepsilon}\rho \mu_t \left(\frac{\varepsilon}{k}\right) - C_{2\varepsilon}\rho \frac{\varepsilon}{k} \quad (3)$$

where k is the turbulent kinetic energy, ε its dissipation rate, and μ_t is turbulent viscosity.

3. Methodology

The first phase was analyzing the morphological traits of the Peregrine Falcon and Albatross in order to get important aerodynamic properties. A 3D wing model was then created using SolidWorks and numerically simulated using ANSYS Fluent. The resultant aerodynamic performance was then evaluated in relation to the efficiency and behaviour of a NACA 23015 airfoil-shaped wing. Figure 1 illustrates the numerous phases of the research process, starting with biological observation and concluding with computational analysis.

3.1 Airfoil Geometry and Parameters

The albatross's wide wingspan [8] sets it apart and enhances its ability to glide. Its high aspect ratio [4] causes the wing tips to taper, which lessens the produced drag. As a result, a wing design with tapered tips and a width of 1.2 meters was created. The root chord length was 0.4 m, and the tip chord length was 0.2 m when the taper ratio was set at 0.5. In contrast, depending on its actions, the Peregrine Falcon exhibits a range of sweep angles during flight, from 40° to 90° [9]. The Peregrine Falcon's greatest and minimum sweep angles are shown in Figure 2. But, as shown in Figure 3, the Albatross usually keeps its sweep angle smaller. The current design used a sweep angle of 20° to mimic actual gliding circumstances. The design approach took into consideration the fact that birds are known to be able to dynamically modify their sweep angle in response to flight conditions. Both bird species use a dihedral wing shape to maintain stability during gliding flight [5].

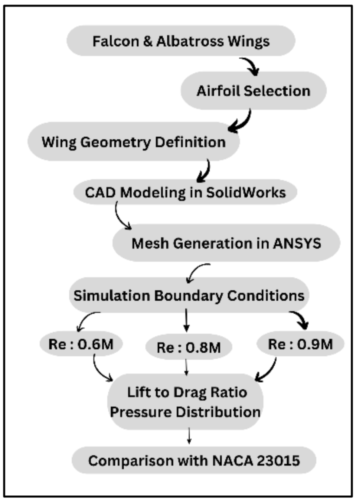

Fig.1 Methodology

As a result, the model contained a dihedral angle of 5°. Aluminium 6061 was used to create the wings because of its advantageous qualities of low density, high strength, and corrosion resistance. All of the geometric characteristics for the albatross and falcon-inspired wings are summarized in Table 1.

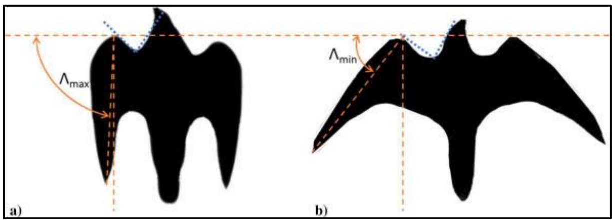

Fig.2 The Wing of Peregrine Falcon [9]

Fig.3 The wing of Albatross [4]

Table 1 Dimensions

Sl. No	Parameters
1	Wing span 1.2 m
2	Root chord 0.4 m
3	Tip chord 0.2
4	Tapper Ratio 0.5
5	Thickness to Chord ratio root 12% & Chord 8%
6	Sweep angle 20 degree
7	Dihedral angle 5 degree
8	Material Aluminum 6061

3.2 CAD Modelling

SOLIDWORKS was used to build the wing shape in accordance with the given dimensions. The two-dimensional aerofoil designs were made using the spline tool, and the three-dimensional wing structure was formed by connecting them with Plane and lofted boss/base features.

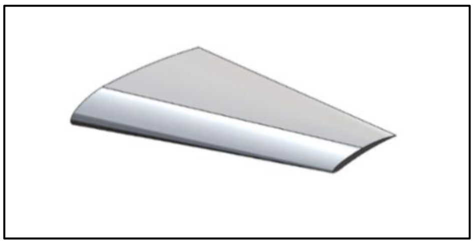

Fig.4 Designed A&F Wing

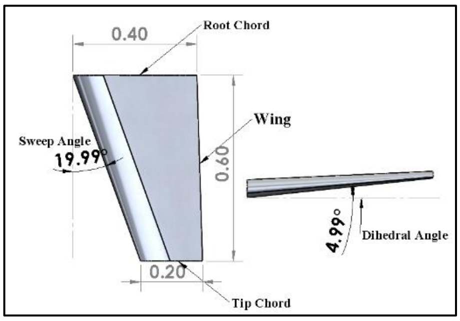

Fig.5 Wing dimensions

The bio-inspired wing was evaluated in comparison to a wing that resembled the NACA 23015 aerofoil. The geometry was constructed using a root chord length of 0.4 meters and a tip chord length of 0.2 meters using the coordinate data for the NACA 23015 profile.

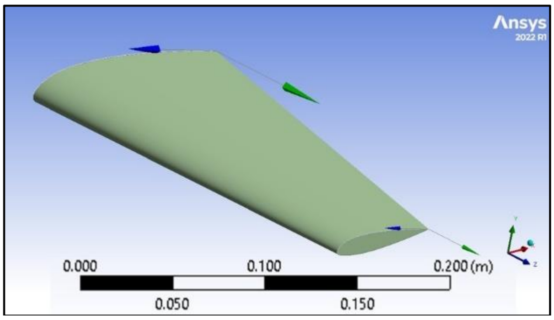

Fig.6 NACA 23015 wing

3.3 Simulation Setup

ANSYS Fluent within the Fluid Flow (Fluent) analytical framework was used to conduct the numerical analysis. Using the same boundary conditions and solver settings for consistency, the simulation started with the NACA 23015 airfoil-shaped wing and then moved on to the bio-inspired wing. After importing the drawings into DesignModeler, a rectangular flow domain was created to depict the surrounding airflow.

The computational analysis was carried out at a Reynolds number of 6×10^5, using air properties that correspond to sea-level conditions, specifically, a kinematic viscosity of 1.802×10^{-5} m²/s and a density of 1.225 kg/m³. The control volume was defined using a velocity inlet and a pressure outlet as boundary conditions. The simulation was run for 2000 iterations in order to verify that the solution had reached convergence. Tables 2, 3, and 4 provide specifics on the boundary conditions, flow conditions, and meshing parameters, respectively. A sub-sonic wind tunnel [10] can be used to validate the full-span model (1.2 m) with the specified geometry made from Aluminum 6061. A six-component balance can be used to quantify the lift and drag coefficients while evaluating the wing at different angles of attack at matching Reynolds numbers in a low-turbulence environment. Separation and tip vortex behaviour can be detected with the aid of surface flow visualisation. In comparison to traditional aerofoils, the biomimetic design is anticipated to exhibit delayed stall characteristics and attain higher lift-to-drag ratios. Data reliability will be improved by carrying out comprehensive uncertainty analysis and repeatability testing, which will provide future researchers with a solid approach to duplicate and build upon this validation.

Table 2 Mesh Properties

Sl. No	Parameters	Value
1	Type	Unstructured mesh
2	No. of nodes	343747
3	No. of cells	1090105
4	Minimum edge length	2.3418×10^{-2} m
5	Inflation layer	12

Table 3 Boundary Conditions

Sl. No	Parameter	Value
1	Physics	K-ω SST model
2	Inlet Type	Velocity inlet
3	Inlet Velocity	29.78 m/s
4	Outlet type	Pressure Outlet
5	Time Dependency	Steady State
6	Algorithm	Coupled
7	Slover	Pressure Based
8	Spatial Discretization	Second-order Upwind scheme
9	Compressibility	Incompressible

Table 4 Flow Conditions

Sl. No	Parameters	Flow Condition
1	Viscosity	1.802×10^{-5}
2	Air Density	1.225 Kg/m³
3	Reynolds Number	609000
4	Condition	Far Field
5	Altitude	Sea level
6	Operating Pressure	101325 Pa
7	Operating Temperature	288.16 k

4. Result and Discussion

In this analysis, the impact of varying the angle of attack (AoA) was investigated and each cases was carried out at the same velocity 29.78 m/s and same Re of $\mathbf{6 \times 10^5}$. The angle of attack ranges from $\mathbf{-10° \text{ to } 35°}$.
A study is conducted to evaluate the aerodynamic efficiency of the wings depicted in **Fig. 4** and **Fig. 6.**. The numerical (using Ansys Fluent) results of lift and drag coefficient are plotted and compared in **Fig.7.**

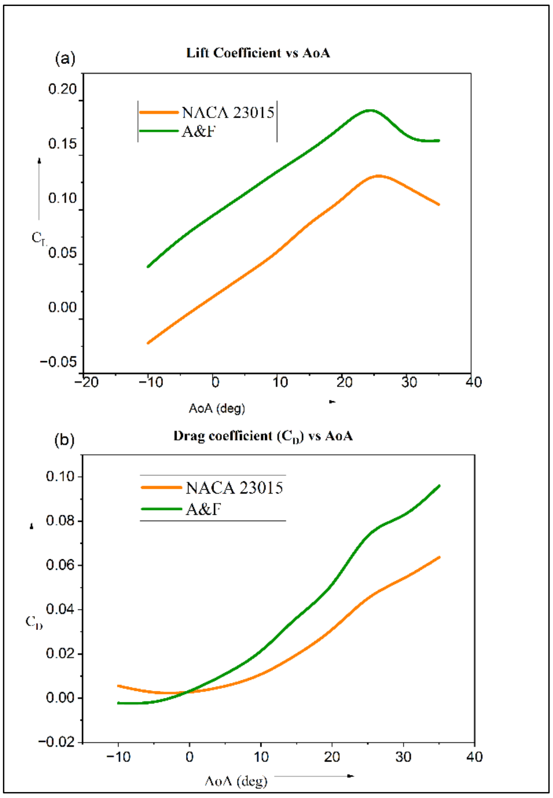

Fig. 7 Examination of the variations in lift coefficient and drag coefficient as the angle of attack changes for A&F and NACA 23015 wings

For A&F Wing, the lift coefficient increases steadily at lower angles of attack, indicating efficient lift generation even at low angles. The wing achieves a higher peak $\mathbf{C_L}$, suggesting superior lift capabilities compared to the NACA 23015 wing. The $\mathbf{(C_L)_{max}}$ occurs at a significantly higher $\boldsymbol{\alpha}$ ranges from $\mathbf{21^{\circ}}$ to $\mathbf{25^{\circ}}$(the stall angle), indicating a delay in stall behaviour. This delayed stall shows the emphasize aerodynamic stability and maneuverability of A&F wing in steep-angle applications [11].

For NACA 23015 Wing, the $\mathbf{C_L}$ increases almost linearly with $\boldsymbol{\alpha}$ up to a certain angle which is also varies from $\mathbf{21^{\circ}}$ to $\mathbf{26^{\circ}}$, beyond which $\boldsymbol{C_L}$ rapidly declined due to flow separation, indicating stall.

For similar $\boldsymbol{\alpha}$, A&F wing generates more lift compared to NACA 23015, showing that the A&F wing design has more operating range in terms of lift generation especially at higher $\boldsymbol{\alpha}$, which hold natural optimizations found in the wings of the albatross for gliding and falcon for high-speed maneuvers.

For A&F Wing, the $\boldsymbol{(C_D)_{min}}$ appears on the $\boldsymbol{\alpha}$ = - $\mathbf{6^{\circ}}$ as can be observed from **Fig 7**, it is evident that the A&F wing is optimized for efficient sailing with minimized energy consumption. With the increased $\boldsymbol{\alpha}$, the $\boldsymbol{C_D}$ rises steadily, due to the increased resistance associated with higher $\boldsymbol{\alpha}$. However, the A&F wing shows a slightly higher drag than the NACA 23015 wing across most of the $\boldsymbol{\alpha}$ range.

For NACA 23015 Wing, the $\boldsymbol{C_D}$ starts low at lower $\boldsymbol{\alpha}$ but increases rapidly with increasing $\boldsymbol{\alpha}$, similar to the A&F wing. This comparison of $\boldsymbol{C_L}$ and $\boldsymbol{C_D}$ corresponding to diffenrent angles of attack ($\boldsymbol{\alpha}$) demonstrate enhanced aerodynamic performance of A&F wing.

The A&F wing exhibits a steady and reliable L/D ratio throughout most of the α range, with α = 5° demonstrating the highest aerodynamic efficiency, as illustrated in **Fig. 8**. As the $\boldsymbol{\alpha}$ increases, A&F wing shows minimum fluctuations in L/D, even at higher $\boldsymbol{\alpha}$ values, indicating smooth airflow along the wing surface, reducing flow separation with balancing the lift and drag.

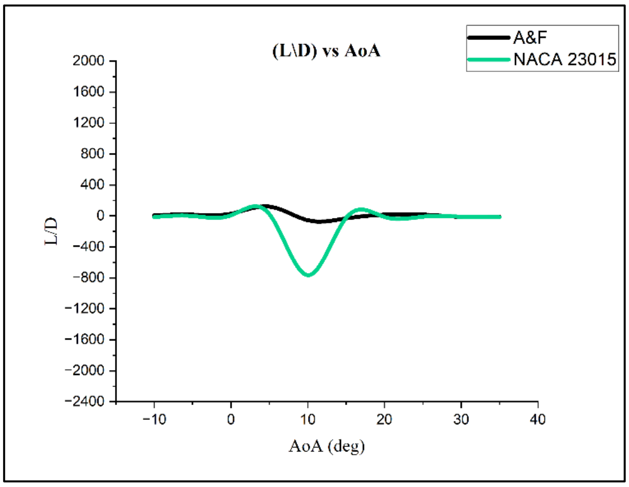

Fig. 8 Comparison of the variation in lift-to-drag ratio (L/D) across varying angles of attack for A&F and NACA 23015 wing.

Table 5 Attainment of maximum aerodynamic efficiency.

SL. No	Wing	$\boldsymbol{\alpha_{(\frac{L}{D})max}}$ (deg)
1	A&F	5
2	NACA 23015	15

The distribution of pressure is visualized in Fig. 9 for varying angles of attack ($\boldsymbol{\alpha}$) = $\mathbf{-10^{\circ}}$ to $\mathbf{35^{\circ}}$for the SST $\boldsymbol{k-\omega}$ turbulence model. Higher-pressure regions, typically found on the lower surface of the wing, signifying with colors (yellow and red), while lower-pressure zones, particularly on the upper surface where lift is generated (green and blue colors).

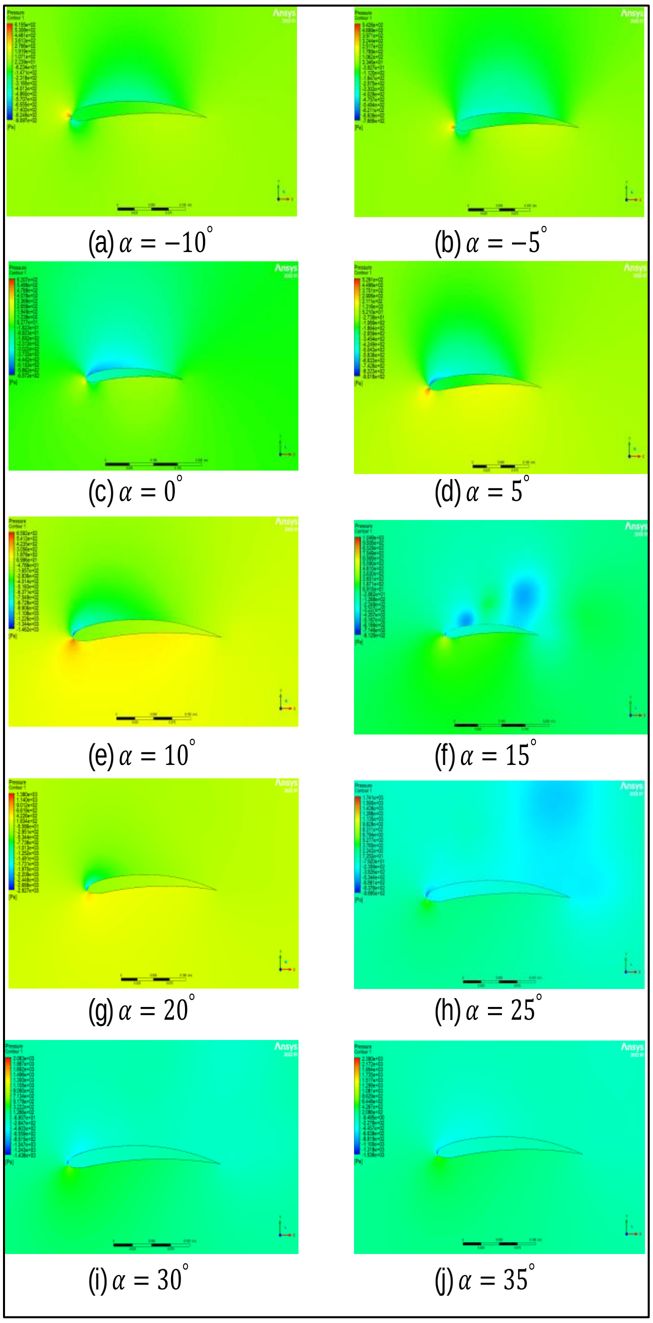

Fig.9 Pressure contours for different angles of attack of A&F wing, employing the SST k-ω model.

Flow starts to separate when angle of attack, $\boldsymbol{\alpha}$ reaches to the value of 15. Over α = $\mathbf{25}^{\circ}$, significant turbulence coupled with pressure losses suggest the onset of stall, see **Fig.9.** At lower angles of attack (e.g. near $\mathbf{0}^{\circ}$), the differential pressure across the upper and lower surfaces of the wing is relatively small. Flow starts to separate when angle of attack, $\boldsymbol{\alpha}$ reaches to the value of $\mathbf{35}^{\circ}$, see **Fig. 10.**

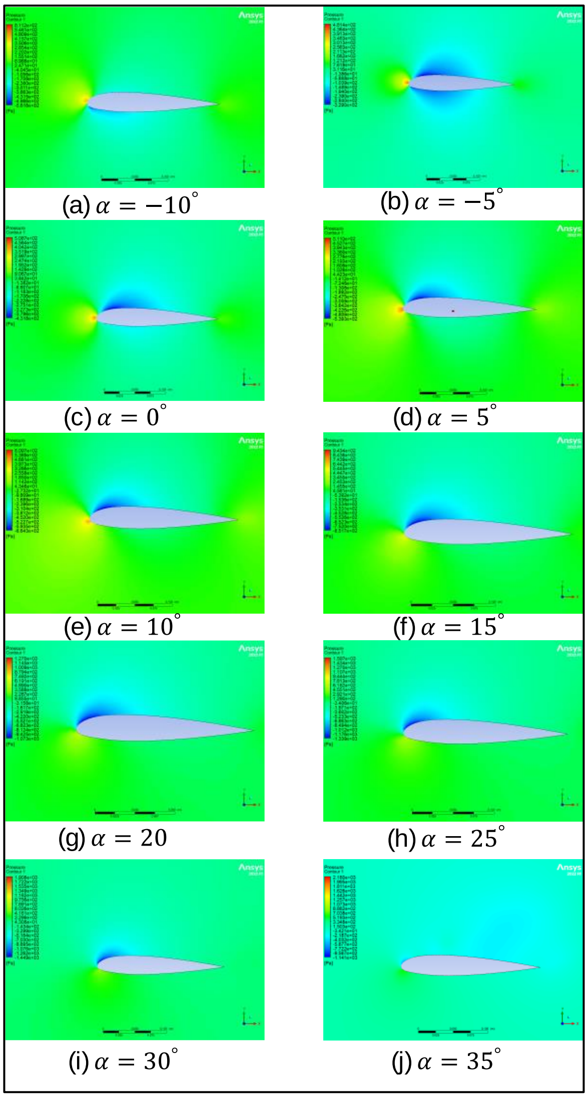

Fig.10 Pressure contours for different angles of attack of NACA 23015 wing, employing the SST k-ω model.

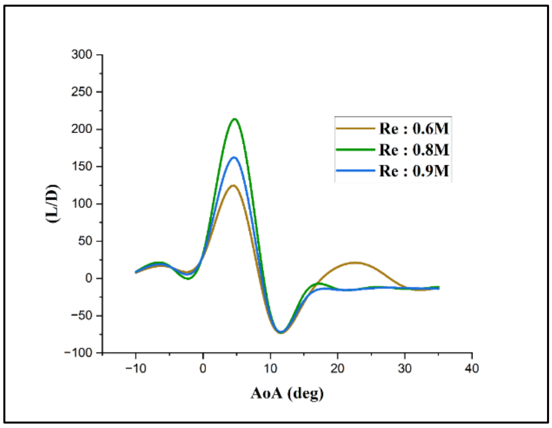

Fig.11 The Lift-to-Drag ratio changes with different angles of attack for the A&F across various Reynolds numbers

Table 6 Changes in A&F's performance metrics at various Reynolds numbers.

Parameters	Re: 6×10^5	Re: 8×10^5	Re: 9×10^5
$(\frac{L}{D})_{max}$	121.598	212.0251	160.184
$(C_L)_{max}$	0.191	0.183	0.193
$(C_D)_{min}$	-0.0022211	-0.00318	-0.00291

Fig.11. depicts $(\frac{L}{D})$ with the angle of attack. The $(\frac{L}{D})_{max}$, $(C_L)_{max}$ are attained at small $\alpha = 5^{\circ}$, for all the values of Re of 6×10^5, 8×10^5, 9×10^5. The $(C_D)_{min}$ are attained at $\alpha = -10^{\circ}$.

Previous Study on from peregrine FALCON airfoil shows[1] lower $(\frac{L}{D})_{max} = 84.24$,$(C_D)_{min} = 0.0129$ as compared to our findings for A&F wing at Re = 6×10^5, see table 6.

The higher lift coefficient, C_L of the A&F wing at low to moderate angles of attack and its delayed stall behavior indicate two practical benefits for UAVs and gliders. It can produce more lift for the same wing area, which may improve payload capacity and flight endurance and also the delayed stall provides a greater safety margin and better control during high-angle maneuvers.

However, There are a number of structural and material challenges when implementing the Albatross Falcon inspired wing design in full-scale aircraft or unmanned aerial vehicles. Due to greater bending forces at the root, the high-aspect-ratio wing [12-13] (1.2 m span, 0.4 m root chord, and 0.2 m tip chord) may require more reinforcing, increasing structural weight and decreasing efficiency. The structure is more susceptible to aeroelastic problems including flutter and torsional deformation due to the 20° sweep angle and 5° dihedral, which also complicate load distributions.

Although aluminium 6061 is strong and resistant to corrosion, its fatigue life and buckling resistance might not be sufficient for the thin design when compared to more sophisticated composites. For the tapered, pointed tip design to provide the best aerodynamic performance, exact geometric tolerances must be achieved.

At full scale, issues like vibration control, maintenance access, and Reynolds number effects become more significant, highlighting the necessity of aeroelastic optimisation and potentially switching to lighter, stiffer materials.

5. Conclusion

This study investigated a biomimetic wing design inspired by the flight mechanics of the Albatross and Peregrine Falcon, comparing its aerodynamic performance to that of the NACA 23015 airfoil. The result indicate that the A&F wing offers improved lift generation, increased stall resistance, and superior aerodynamic efficiency across a range of angles of attack by combining crucial elements from both birds, such as a high aspect ratio, ideal sweep angle, and dihedral angle Because of these qualities, it is especially well-suited for applications that call for both high speed manoeuvrability and effective glide.

The results show that bioinspired wing designs can greatly improve aircraft performance, particularly in areas that are crucial for fuel efficiency and flying stability. In order to further improve wing performance under various flight conditions, future study may examine the incorporation of adaptive morphing technology. This research advances more advanced, sustainable, and effective aviation designs by taking inspiration from nature.

7. References

[1] S. Yuvaraj, A. Adithya, G. Banu, and S. Srithar, "Numerical and experimental investigation of airfoil derived from peregrine FALCON," *Measurement: Sensors*, vol. 31, no. October 2023, p. 100956, 2024, doi: 10.1016/j.measen.2023.100956.

[2] P. L. Richardson, E. D. Wakefield, and R. A. Phillips, "Flight speed and performance of the wandering albatross with respect to wind," *Movement Ecology*, vol. 6, no. 1, pp. 1–15, 2018, doi: 10.1186/s40462-018-0121-9.

[3] B. Ponitz, A. Schmitz, D. Fischer, H. Bleckmann, and C. Brücker, "Diving-flight aerodynamics of a peregrine falcon (Falco peregrinus)," *PLoS ONE*, vol. 9, no. 2, 2014, doi: 10.1371/journal.pone.0086506.

[4] B. C. Mathew, J. V. M. Lal Jeyan, P. Dutta, and R. R. Savale, "Evolutionary and Hereditary Traits of an Albatross and its Aerodynamic Optimality," *IOP Conference Series: Earth and Environmental Science*, vol. 775, no. 1, 2021, doi: 10.1088/1755-1315/775/1/012002.

[5] H. Zhang, S. Zhang, and T. Xiang, "Effects of Bio-Inspired Wing Dihedral Variations on Dynamic Soaring Performance of Unmanned Aerial Vehicles," *Drones*, vol. 8, no. 11, 2024, doi: 10.3390/drones8110623.

[6] A. Kulshreshtha, S. K. Gupta, and P. Singhal, "FEM/CFD analysis of wings at different angle of attack," *Materials Today: Proceedings*, vol. 26, no. July, pp. 1638–1643, 2019, doi: 10.1016/j.matpr.2020.02.342.

[7] J. V. N. de Sousa *et al.*, *On the Study of Autonomous Underwater Vehicles by Computational Fluid-Dynamics*, vol. 10, no. 01. 2020. doi: 10.4236/ojfd.2020.101005.

[8] J. P. Barnes, "How flies the albatross - the flight mechanics of dynamic soaring," *SAE Technical Papers*, no. 724, 2004, doi: 10.4271/2004-01-3088.

[9] O. Selim, E. R. Gowree, C. Lagemann, E. Talboys, C. Jagadeesh, and C. Brücker, "Peregrine Falcon's Dive: Pullout Maneuver and Flight Control Through Wing Morphing," *AIAA Journal*, vol. 59, no. 10, pp. 3979–3987, 2021, doi: 10.2514/1.J060052.

[10] B. Duan, J. Liu, S. Wang, Z. Chen, and B. Ju, "Wind Tunnel Experimental Study on the Flight Parameters of a Bio-Inspired Bat-like Flapping-Wing Robot," *Aerospace*, vol. 12, no. 7, 2025, doi: 10.3390/aerospace12070615.

[11] X. Bai, H. Zhan, and B. Mi, "Unsteady Aerodynamic Design of a Flapping Wing Combined with a Bionic Wavy Leading Edge," *Applied Sciences*

(Switzerland), vol. 13, no. 3, 2023, doi: 10.3390/app13031519.

[12] P. L. Richardson, “How do albatrosses fly around the world without flapping their wings?,” *Progress in Oceanography*, vol. 88, no. 1–4, pp. 46–58, 2011, doi: 10.1016/j.pocean.2010.08.001.

[13] E. R. Gowree, C. Jagadeesh, E. Talboys, C. Lagemann, and C. Brücker, “Vortices enable the complex aerobatics of peregrine falcons,” *Communications Biology*, vol. 1, no. 1, pp. 1–7, 2018, doi: 10.1038/s42003-018-0029-3.

7. Nomenclature

Symbol	*Meaning*	*Unit*
A&F	Albatross and Falcon	--
AoA	Angle of Attack	Degree
α	Angle of Attack	Degree
Re	Reynolds Number	--
C_L	Lift Coefficient	--
C_D	Drag Coefficient	--
(L/D)	Lift to Drag Ratio	--